Ray-tracing simulations of liquid-crystal gradient-index lenses for three-dimensional displays

Maarten Sluijter,[1,*] Angie Herzog,[1] Dick K. G. de Boer,[1] Marcel P. C. M. Krijn,[1] and H. Paul Urbach[2]

[1]*Philips Research Europe, High Tech Campus 34, MS 31, 5656 AE Eindhoven, The Netherlands*
[2]*Department of Imaging Science and Technology, Optics Research Group, Delft University of Technology, Lorentzweg 1, 2628 CJ Delft, The Netherlands*
[*]*Corresponding author: Maarten.Sluijter@philips.com*

Received June 26, 2009; revised August 6, 2009; accepted August 26, 2009;
posted September 10, 2009 (Doc. ID 113403); published October 9, 2009

For the first time, to our knowledge, we report ray-tracing simulations of an advanced liquid-crystal gradient-index lens structure for application in switchable two-dimensional/three-dimensional (3D) autostereoscopic displays. We present ray-tracing simulations of the angular-dependent lens action. From the results we conclude that the lens action of the advanced optical design corresponds to the desired performance for small viewing angles. For oblique viewing angles of approximately 30° and higher, the lens action becomes significantly weaker compromising the 3D performance of an autostereoscopic display. The general approach and the advanced ray-optics analysis procedures presented form a useful tool in the search for improvements for high viewing angles and enable a better understanding of the liquid-crystal technology discussed.

OCIS codes: 080.3095, 160.1190, 260.1440.

1. INTRODUCTION

An attractive technology for autostereoscopic three-dimensional (3D) displays is based on LCDs equipped with an array of cylindrical lenses, called a lenticular. These types of 3D displays project distinct images (views) to each eye of a viewer without a loss in brightness, generating the binocular disparity and motion parallax depth cues [1]. The principle of operation of a multiview lenticular-based 3D display is shown in Fig. 1. In 2004, an innovative technique has been developed for creating autostereoscopic 3D images by combining a multiview lenticular-based 3D display technology with advanced computer graphics and image rendering techniques [2]. The display technology involved makes use of a switchable liquid-crystal-based lenticular enabling switching between a conventional two-dimensional (2D) mode and an autostereoscopic 3D mode [3,4]. The switchable lenticular is an array of negative lenses filled with liquid crystal. The liquid crystal can be switched between two optical states with the help of an electric field. As a result, the lens action of the lenticular can be switched on and off. In this way it is possible to have a high-brightness 3D display capable of regaining the full native 2D resolution of the underlying display.

Another attractive route to enable the switchable lens effect in a 3D display is the use of a liquid-crystal gradient-index (GRIN) lens structure [5,6]. A GRIN lens has a lens action due to gradients in the material properties rather than a physically curved surface. Then a lenticular is no longer required, resulting in size reduction.

In contrast to isotropic lenses, the lens effect of a liquid-crystal GRIN lens is difficult to model. First, the inhomogeneous liquid-crystal profile needs to be simulated by minimizing the free energy, which can be done using software programs such as LCD Master [7] or 2dimMOS [8]. Then the optical properties of the obtained liquid-crystal profile are investigated by, for example, ray-tracing simulations. This means that the optical design of a liquid-crystal GRIN lens involves a complex process characterized by trial and error. In this paper, we will investigate the issues involved for the GRIN solutions in 3D displays.

Pioneering studies on liquid-crystal GRIN lenses were done in the 1970s by Sato [9] and Berreman [10]. GRIN lenses based on liquid crystal appear in many forms and form a subject widely discussed in the literature [11–16]. There are many methods available to calculate the optical properties of liquid-crystal GRIN lenses. For example, in [17] a ray-tracing algorithm is introduced to trace ray paths in inhomogeneous uniaxially anisotropic media and applied to a liquid-crystal lens. Although the so-called ray-bundle method discussed appears to be accurate, the ray-tracing procedure involves a complicated process when compared with the Hamiltonian principle discussed by Kline and Kay [18]. The Hamilton equations (based on the Hamiltonian principle) for ray tracing in inhomogeneous uniaxially anisotropic media are thoroughly discussed in the paper by Sluijter *et al.* [19]. Another simple but effective method is the so-called Huygens method based on the Huygens principle [20], although it does not fully take into account the inhomogeneous properties of the liquid-crystal material. In this paper, we will apply

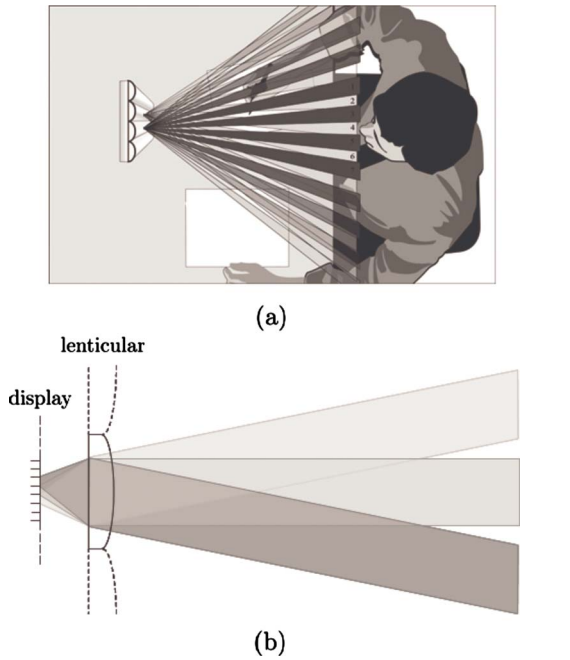

Fig. 1. (Color online) Schematic principle of an autostereoscopic lenticular-based 3D imaging display. In (a), multiple images are projected to multiple viewing directions. The neighboring images form stereo pairs, thus enabling the binocular disparity and motion parallax depth cues. The lenticular is placed in front of a display as depicted in (b). The light from subpixels of the display is collimated by the lenticular and directed toward different viewing directions. The contribution of all pixels of a display produces the individual views.

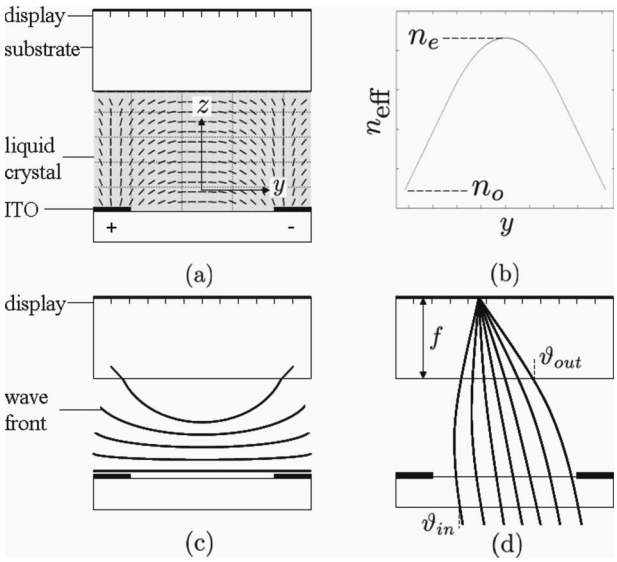

Fig. 2. Schematic working principle of a liquid-crystal GRIN lens integrated in a 3D display. (a) shows a liquid-crystal layer between two transparent substrates. The figure shows one unit cell, which is repeated in the y direction (see also Fig. 1). An ITO electrode structure induces an electric field along which the liquid-crystal molecules align (indicated by the black stripes). In (b), we show how the effective index of refraction typically varies with position between n_o and n_e, with $n_e > n_o$. The propagating wavefront of an incident plane wave (polarized in the yz plane) is depicted in (c). The ray paths that correspond to these wavefronts are depicted in (d), but this time for a plane wave with an angle of incidence ϑ_{in}. Ideally, the ray paths focus at a distance f in the pixel plane of the display.

geometrical optics and use ray-tracing techniques to model the propagation of light in inhomogeneous anisotropic media.

The liquid-crystal GRIN lenses discussed by Kraan *et al.* [20] form a different type of lens (beam-steering lens) than the one used in 3D displays. Moreover, light at normal incidence was considered, while the angular-dependent behavior of a liquid-crystal GRIN lens is important, in particular for autostereoscopic multiview 3D displays.

In this paper, we will focus our attention to two different approaches to model liquid-crystal GRIN lenses: the Huygens and the Hamiltonian principles. We will apply both principles to investigate the angular-dependent optical properties of an advanced liquid-crystal GRIN lens structure for application in 3D displays.

2. LIQUID-CRYSTAL-BASED GRIN LENS

A liquid-crystal-based GRIN lens is an optical system that enables a lens effect due to an imposed gradient in the director profile of a liquid-crystal layer. The director is defined as the local direction of the optical axis. In what follows, we discuss the optical design of an advanced liquid-crystal GRIN lens for application in multiview autostereoscopic switchable 3D displays.

A. Working Principle

Figure 2(a) shows a schematic cross section of a liquid-crystal GRIN lens integrated in a 3D display. The optical configuration consists of two parallel transparent substrates with a liquid-crystal layer in between placed in front of a display. The distance between the lenses and the pixel plane of the display should be approximately the focal length of the lenses [see also Fig. 1(b)]. Both substrates are provided with a rubbed polyimide (PI) layer to obtain a preferred alignment of the liquid-crystal material in the absence of an electric field: the y direction. One of the substrates is provided with a transparent indium tin oxide (ITO) electrode structure consisting of line electrodes with their long axis in the x direction. When a voltage is applied to the electrodes, there is an electric field inside the liquid-crystal layer in the yz plane. As a consequence, the liquid-crystal molecules align along the (curved) electric field lines, occupying the lowest possible energy state. As a result, there is a gradient in the liquid-crystal profile.

When a collimated beam of light (polarized in the yz plane) enters the liquid-crystal layer, light rays converge since we consider a liquid crystal for which $n_e > n_o$, where n_o and n_e are the ordinary and extraordinary refractive indices, respectively. To understand this, we consider the effective index of refraction for propagation in the vertical z direction. Figure 2(b) shows how the effective index of refraction n_{eff} typically varies with the position y. An incident plane wavefront is transformed to a curved wavefront as can be seen in Fig. 2(c). Since $n_e > n_o$, the portion of the wavefront in the center of the lens is delayed with respect to portions of the wavefront further away from the center. Then light rays are converging toward a focal point. Figure 2(d) shows the ray paths of an incident plane wave with an angle of incidence ϑ_{in}. For a perfect

collimation of the views, all light rays intersect at the focal distance f in the pixel plane of the display and then the angle of refraction ϑ_{out} satisfies

$$\tan \vartheta_{\text{out}} = \frac{y}{f}, \tag{1}$$

where $y=0$ is defined at the center of the lens. Note that, if $\vartheta_{\text{out}} \ll 1$, it is a linear function of the position y.

B. Experimental Results of a Liquid-Crystal GRIN Lens Structure

A schematic cross section of the liquid-crystal GRIN lens structure discussed in this paper is depicted in Fig. 3. This advanced optical design of the GRIN lens structure (patented in [21]) is based on the results of recent studies on GRIN lenses (cf. [5], p. 852). One important issue is that in the neighborhood of the electrodes the liquid crystal does not align properly along the electric field lines. Hence the liquid crystal in these particular regions does not contribute to the desired lens action. The region contributing to the lens action can be increased if (1) the distance between the line electrodes and the liquid-crystal layer is increased by adding an extra dielectric transparent layer and (2) a grounded ITO electrode layer is added parallel to the electrode wire structure on top of a second dielectric transparent layer (see Fig. 3). These features improve the electric field distribution inside the liquid-crystal layer and thus the lens performance [5,21]. The relative dielectric permittivity of the two additional dielectric layers should be in the range of common glass ($3.0 \le \varepsilon_r \le 5.0$). In addition, for a lens pitch of 166 μm, the thickness of the two dielectric layers should be of the order of 50 μm. The width of the ITO electrodes is 10 μm.

With the advanced optical design discussed above, the active region is approximately 60% of the lens pitch (100 μm) with a focal distance f of approximately 1.8 mm in glass. Then the optical properties are close to the desired performance for application in an autostereoscopic 3D display.

The angle of refraction ϑ_{out} [see Eq. (1)] for light at normal and oblique angles of incidence has been measured in an experiment. In the experimental setup, a focused laser beam scans the lens pitch of a GRIN lens (in the y direction of Fig. 2). The spot size in the waist of the focused laser beam is 24 ± 5 μm. Then the position and the intensity of the refracted laser light are detected by a CCD camera. From these data the desired angle of refraction

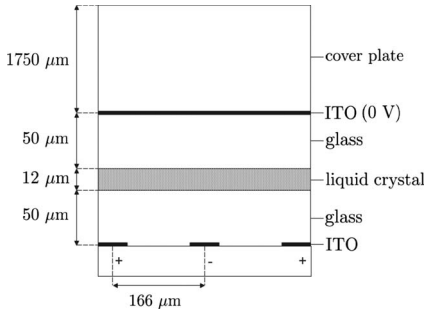

Fig. 3. Schematic cross section of the advanced optical design of a liquid-crystal GRIN lens structure [21]. The liquid-crystal mixture that is used is TL213, for which $n_o = 1.5271$ and $n_e = 1.7659$.

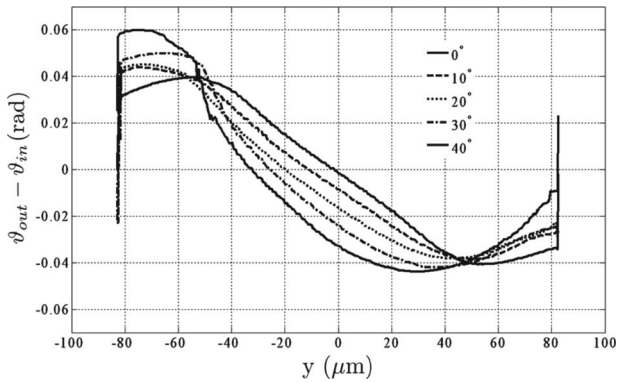

Fig. 4. Measured angle of refraction $\vartheta_{\text{out}} - \vartheta_{\text{in}}$ (in air) as a function of the position y for the GRIN lens defined in Fig. 3 for $\vartheta_{\text{in}} = 0° - 40°$. For $\vartheta_{\text{in}} = 0°$ in the region where $|y| \le 45$ μm, ϑ_{out} is a linear function of y: $\vartheta_{\text{out}} = -0.85$ mrad/μm. In the region where $|y| > 45$ μm, ϑ_{out} is not linear.

ϑ_{out} in air is calculated. These measurements will be discussed to show the working principle and provide a reference for the lens action for light at normal incidence.

Figure 4 shows the measured angle of refraction ϑ_{out} (in air) as a function of position for an angle of incidence $\vartheta_{\text{in}} = 0°$. In the experiment a voltage of approximately 100 V (AC) is applied to the electrodes. From the figure we can see that, in the region where $|y| \le 45$ μm, ϑ_{out} is approximately a linear function of y. This result is in agreement with Eq. (1) since $\vartheta_{\text{out}} \ll 1$ rad. The linearity of ϑ_{out} for normal incidence ($\vartheta_{\text{in}} = 0°$) is $\vartheta_{\text{out}} = -0.85$ mrad/μm. In the region where $|y| > 45$ μm, ϑ_{out} is inaccurate because close to the electrodes light is scattered in various directions. For simplicity, the angle ϑ_{out} at normal incidence will be approximated by an average: $\vartheta_{\text{out}} = \pm 38.25$ mrad. Figure 4 also shows the experimental results for $\vartheta_{\text{in}} = 10°, \ldots, 40°$ with a step size of 10°. From the results we can conclude that the linearity of ϑ_{out} decreases with increasing ϑ_{in}. Next, we will briefly discuss the Huygens principle applied to a GRIN lens.

3. HUYGENS METHOD

The Huygens principle applied to an anisotropic liquid-crystal layer is derived in the paper by Kraan *et al.* (cf. [20], p. 3468). In this section, we will discuss the basic principle of the Huygens method and refer to the paper of Kraan *et al.* [20] for further details.

In the Huygens method the propagation of light rays in the lateral y direction is assumed to be negligible inside the liquid-crystal layer. This means that, effectively, the thickness of the liquid-crystal layer is assumed to approach zero. This is a fair approximation since the ratio between the thickness and the lens pitch of the liquid-crystal layer is $(\frac{12}{166} =) 0.072$. The method attributes an effective index of refraction to each position y of the liquid-crystal layer. This is achieved by averaging the effective index of refraction $n_{\text{eff}}(y,z)$ over the vertical z direction for each position y. As a result, the Huygens method does not take into account the inhomogeneous material properties in the vertical z direction.

For each position $\mathbf{r}$ inside the liquid crystal there is a director $\hat{\mathbf{d}}(\mathbf{r})$. We assume that the director, the direction of

propagation (indicated by the unit vector $\hat{\mathbf{s}}$), and the polarization of the light are all parallel to the yz plane. Hence light rays inside the liquid crystal are extraordinary. For extraordinary rays, we have

$$n_{\text{eff}}(\mathbf{r},\mathbf{s}) = \sqrt{\frac{n_o^2 n_e^2}{n_o^2[1-(\hat{\mathbf{s}},\hat{\mathbf{d}})^2]+n_e^2(\hat{\mathbf{s}},\hat{\mathbf{d}})^2}}, \tag{2}$$

with $\mathbf{s}=|\mathbf{s}|\hat{\mathbf{s}}=n_{\text{eff}}\hat{\mathbf{s}}$ and $\hat{\mathbf{s}}$ denotes the direction of propagation inside the liquid-crystal layer. For a fixed position y and direction of propagation $\hat{\mathbf{s}}$, we can average the effective index of refraction over the vertical direction z. Then the average effective index of refraction is given by

$$\bar{n}_{\text{eff}}(y) = \frac{1}{h}\int_0^h n_{\text{eff}}(\mathbf{r})\mathrm{d}z, \tag{3}$$

where h is the thickness of the liquid-crystal layer.

Figure 5 shows the geometry of a liquid-crystal GRIN lens with the relevant parameters indicated. We consider an incident plane wave with an angle of incidence ϑ_{in}. The figure shows the Huygens spheres at positions y and $y+\mathrm{d}y$. The Huygens spheres evolve differently at these two positions since the effective index of refraction varies over the distance $\mathrm{d}y$. The emerging plane wave has an angle of refraction ϑ_{out}. A temporal analysis (cf. [20], p. 3468) of the evolution of the Huygens spheres leads to a relation between the angles ϑ_{in} and ϑ_{out} (cf. [20], p. 3469, Eq. (8)),

$$n_{\text{glass}}\sin\vartheta_{\text{out}} = n_{\text{glass}}\sin\vartheta_{\text{in}} + h\frac{\mathrm{d}\bar{n}_{\text{eff}}(y)}{\mathrm{d}y}, \tag{4}$$

where n_{glass} is the index of refraction of the top and bottom glass substrates. The second term on the right side of Eq. (4) is an additional term to Snell's law in the presence of a gradient in the index of refraction in the y direction. In addition, we remark that $\bar{n}_{\text{eff}}(y)$ is a function of ϑ_{in} and $\hat{\mathbf{s}}$. In Section 4, we will use the Huygens method to investigate the angular-dependent properties of the advanced GRIN lens structure.

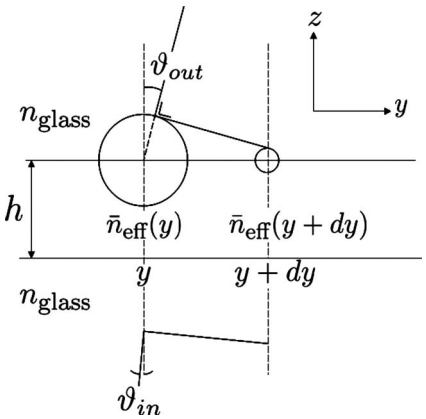

Fig. 5. Evolution of the Huygens spheres in a liquid-crystal layer. The Huygens spheres evolve differently at the positions y and $y+\mathrm{d}y$ since at these positions the averaged effective index of refraction $\bar{n}_{\text{eff}}(y)$ varies over the distance $\mathrm{d}y$. The figure shows an incident plane wave with an angle of incidence ϑ_{in} and the corresponding emerging plane wave with an angle of refraction ϑ_{out}. Here it is assumed that $\bar{n}_{\text{eff}}(y)<\bar{n}_{\text{eff}}(y+\mathrm{d}y)$. The liquid-crystal layer has a thickness h and the indices of refraction of the two glass substrates are indicated by n_{glass}.

4. RAY-TRACING SIMULATIONS BASED ON EXPERIMENTAL RESULTS

In this section, we first calculate the liquid-crystal director profile from the measurement presented in Fig. 4. We will do this with the help of the (reverse) Huygens method discussed in Section 3. Second, using the calculated director profile $\hat{\mathbf{d}}(y)$, we will investigate the angular-dependent optical properties of the GRIN lens structure using the Huygens method.

A. Averaged Director Profile

First, we calculate $\bar{n}_{\text{eff}}(y)$ using Eq. (4) and $\vartheta_{\text{out}}(y)$ for normal incidence. Note that $\vartheta_{\text{out}}(y)$ in Fig. 4 applies in air. Then, with the help of Snell's law, Eq. (4) is rewritten for light at normal incidence ($\vartheta_{\text{in}}=0$) in air ($n_{\text{air}}=1$) as follows:

$$\frac{\sin\vartheta_{\text{out}}(y)}{h} = \frac{\mathrm{d}\bar{n}_{\text{eff}}(y)}{\mathrm{d}y}. \tag{5}$$

The averaged effective index of refraction $\bar{n}_{\text{eff}}(y)$ can be obtained when integrating Eq. (5) on both sides. Then, for $\vartheta_{\text{in}}=0°$, we have

$$\bar{n}_{\text{eff}}(y) = \frac{1}{h}\int_0^y \sin\vartheta_{\text{out}}(y)\mathrm{d}y + n_e, \tag{6}$$

since at the position $y=0$ we have $\bar{n}_{\text{eff}}(0)=n_e$ [see Fig. 2(b)]. Figure 6(a) shows $\bar{n}_{\text{eff}}(y)$ in case $\vartheta_{\text{out}}(y)$ is given by $\vartheta_{\text{out}}(y)=-0.85$ mrad/μm for $|y|\le 45$ μm and $\vartheta_{\text{out}}(y)=\pm 38.25$ mrad (on average) for $|y|>45$ μm. In addition, we consider a liquid crystal with indices $n_o=1.5271$ and $n_e=1.7659$ (TL213 mixture).

Second, we calculate the averaged director $\hat{\mathbf{d}}(y)$ using Eq. (2). Since we consider light at normal incidence, $\hat{\mathbf{s}}$ is in the vertical z direction (both in air and in the liquid-crystal layer). Then the inner product between $\hat{\mathbf{s}}$ and $\hat{\mathbf{d}}(y)$ satisfies $(\hat{\mathbf{s}},\hat{\mathbf{d}})=(\hat{\mathbf{z}},\hat{\mathbf{d}})=\cos\alpha$, with α being the angle between the vertical direction $\hat{\mathbf{z}}$ and the director $\hat{\mathbf{d}}$. Hence for a certain value of $\bar{n}_{\text{eff}}$ we calculate the corresponding value for α satisfying Eq. (2). The calculation is performed numerically with the Newton–Raphson method (cf. [22], p. 355). The result is depicted in Fig. 6(b). Then the averaged director is given by $\hat{\mathbf{d}}(y)=(0,\sin\alpha,\cos\alpha)$.

B. Huygens Method

With the help of the director profile $\hat{\mathbf{d}}(y)$ [see Fig. 6(b)] and the Huygens method, we calculate the angle $\vartheta_{\text{out}}(y)$ in air for an incident plane wave at different angles of incidence ϑ_{in}. Note that the position y indicates the position where the light enters the liquid-crystal layer between two line electrodes. Figure 7 shows the result for $\vartheta_{\text{in}}=0°,\ldots,60°$ with steps of 10°. As expected, the simulated and the experimental $\vartheta_{\text{out}}(y)$'s (see Fig. 4) match perfectly for $\vartheta_{\text{in}}=0°$. This is because the averaged director $\hat{\mathbf{d}}(y)$ used in the simulations is derived from the Huygens method itself. The comparison of the Huygens method

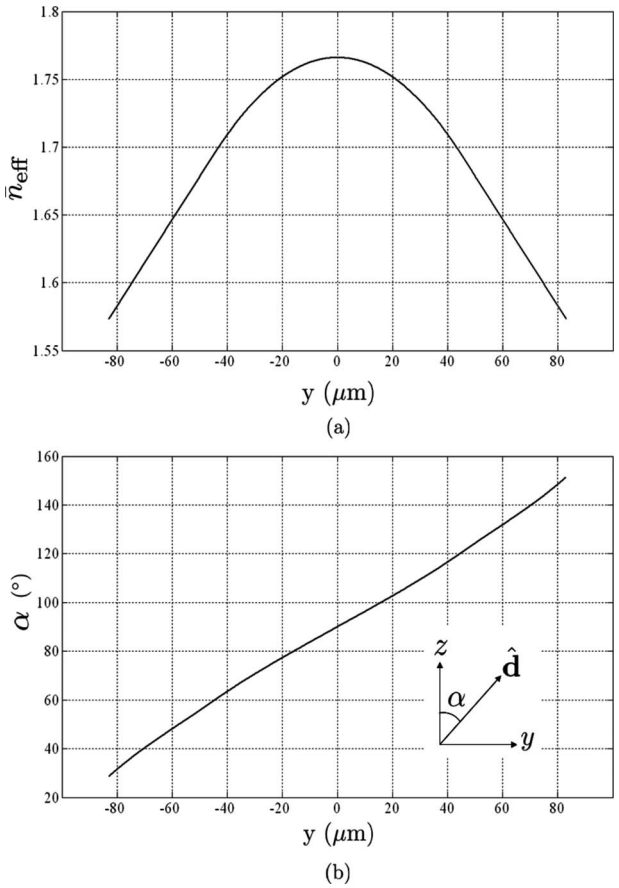

Fig. 6. (a) $\bar{n}_{\mathrm{eff}}$ as a function of y calculated from the experimentally obtained result for $\vartheta_{\mathrm{in}}=0°$ depicted in Fig. 4. At the position $y=0$, the value for $\bar{n}_{\mathrm{eff}}$ is the extraordinary index of refraction $n_e=1.7659$. (b) The angle α (in degrees) between the director $\hat{\mathbf{d}}$ and the vertical z direction (i.e., the direction of propagation $\hat{\mathbf{s}}$) as a function of the position y. Then the director is given by $\hat{\mathbf{d}}=(0,\sin\alpha,\cos\alpha)$.

with experimental results for larger values of ϑ_{in} receives more attention in Section 5. With ϑ_{in} increasing, the linearity of the angle ϑ_{out} with the lateral position y decreases. As a result, the incident light is not focused properly for high values of ϑ_{in}. In other words, the light emerging from the pixel plane of a 3D display is not perfectly collimated as depicted in Fig. 2(d). The imperfections discussed are not a problem for the 3D performance of a 3D display, since a lenticular slightly out of focus with the pixel plane results in a more uniform total angular intensity distribution of a 3D display (cf. [4], p. 3). However, the spot of the focused light beam at the pixel plane should not overlap two neighboring pixels, since then the 3D performance will decrease. In Fig. 7 the lens effect appears to be acceptable for viewing angles less than approximately 30°. This will be discussed further in Section 5.

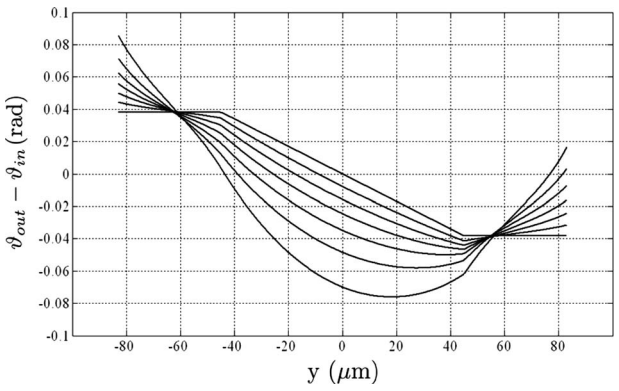

Fig. 7. Ray-tracing results of the Huygens method for $\vartheta_{\mathrm{out}}(y) - \vartheta_{\mathrm{in}}$ for $\vartheta_{\mathrm{in}}=0°,\ldots,60°$ with steps of 10°. Clearly, the linearity of ϑ_{out} decreases with increasing ϑ_{in}.

5. RAY-TRACING SIMULATIONS BASED ON A SIMULATED LIQUID-CRYSTAL PROFILE

In the following exercises, we simulate the director profile to calculate the angular-dependent optical properties of the GRIN lens structure depicted in Fig. 3. The resulting numerical director profile is inhomogeneous in both the y and z directions. In this section, we investigate the angular-dependent behavior of the liquid-crystal lens structure in three different cases: (1) the Hamiltonian principle applied to the simulated director profile $\hat{\mathbf{d}}(y,z)$, (2) the Hamiltonian principle applied to the averaged simulated director profile $\hat{\mathbf{d}}(y)$, and (3) the Huygens method applied to the averaged director profile.

A. Simulated Director Profile

With the definition of the optical configuration depicted in Fig. 3, we simulate the director profile of the liquid-crystal layer between two line electrodes. The director profile is calculated numerically with the optical analysis software program LCD Master [7]. It was found that in the simulations a voltage of 200 V is needed to produce the same lens action as obtained in the experiment at 100 V. The explanation for this is subject to debate. However, the main result here is that we now have a director profile for the specific optical configuration of Fig. 3 that produces a lens action verified by experimental results. The properties of the liquid crystal (TL213 mixture) that we use in the simulations are listed in Table 1. There the values of the elastic constants K_{11}, K_{22}, K_{33}; the static dielectric permittivity $\Delta\varepsilon=\varepsilon_{\parallel}-\varepsilon_{\perp}$; and the viscosity γ of the liquid crystal are indicated. These material properties are important input parameters for the LCD Master program.

The resulting numerical director profile is depicted in Fig. 8(a). Clearly, the director profile is inhomogeneous in both the y and z directions. When we average the director profile over the thickness h of the liquid-crystal layer, we obtain the profile depicted in Fig. 8(b).

Table 1. Liquid-Crystal Properties of TL213 Mixture [23]

Parameter	Value	Parameter	Value
n_o (589 nm)	1.5271	K_{11} (pN)	16.8
n_e (589 nm)	1.7659	K_{22} (pN)	6.5
$\Delta\varepsilon$	5.7	K_{33} (pN)	22.0
γ (cSt)	49		

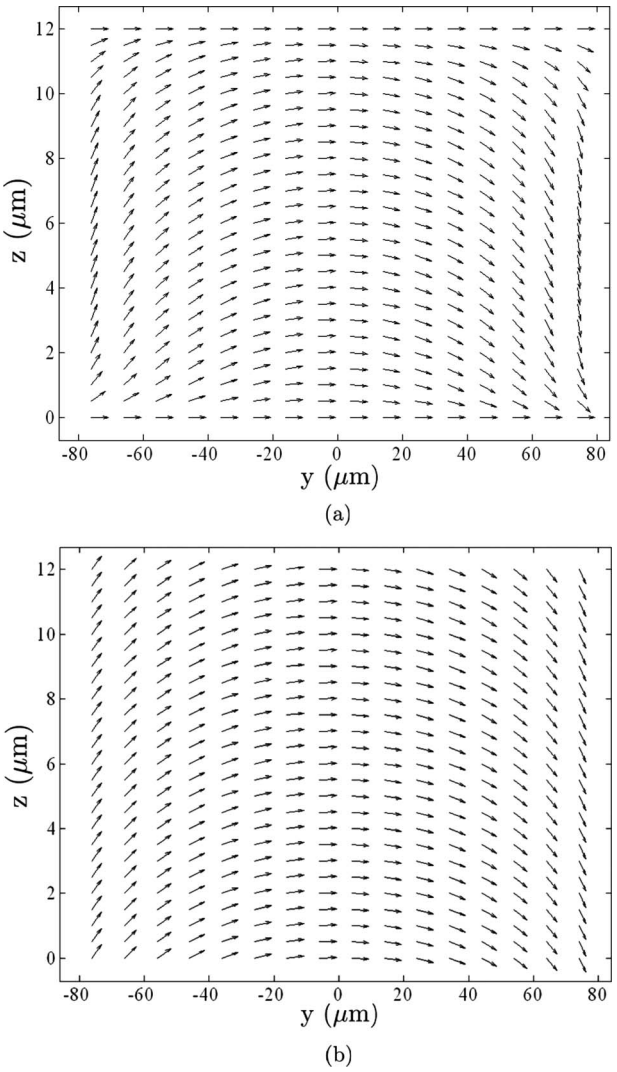

Fig. 8. (a) Simulated director profile $\hat{\mathbf{d}}(y,z)$ of the liquid-crystal layer defined by the optical configuration depicted in Fig. 3. The result is obtained using the simulation program LCD Master [7]. The director profile is inhomogeneous in both the y and z directions and can be used for the Hamiltonian principle. (b) The resulting director profile $\hat{\mathbf{d}}(y)$ when averaged over the vertical z direction.

B. Huygens Method

In this subsection, we apply the Huygens method to the numerical director profile $\hat{\mathbf{d}}(y)$ depicted in Fig. 8(b). First, we calculate the direction of propagation $\mathbf{s}$ in the liquid-crystal layer with the help of the classical theory on anisotropic interfaces summarized in [19] (pp. 1265–1266). Then we use Eqs. (2) and (3) to calculate $\bar{n}_{\text{eff}}(y)$ and apply Eq. (4). Figure 9 shows the result for $\vartheta_{\text{out}}(y)$ for $\vartheta_{\text{in}}=0°,\ldots,50°$, with steps of 10° (dashed curves). The figure also shows the experimental result for $\vartheta_{\text{in}}=0°$. From the figure we conclude that for $\vartheta_{in}=0°$ in the region of $y=0$ μm the slope (angular change per unit length) of $\vartheta_{\text{out}}(y)$ is slightly smaller than the slope of the experimentally obtained result. In other words, the Huygens method predicts a lens effect that is slightly weaker than the lens effect obtained from the experimental characterization.

Finally, Fig. 10 shows the effective index of refraction for various values of ϑ_{in}. Clearly, the maximum of the parabolic curve is shifted to the left for increasing angle of incidence. In fact, the position y in Fig. 10 for which $\bar{n}_{\text{eff}}=n_e$ is equivalent to the position y in Fig. 9 for which $\vartheta_{\text{out}}-\vartheta_{\text{in}}=0$.

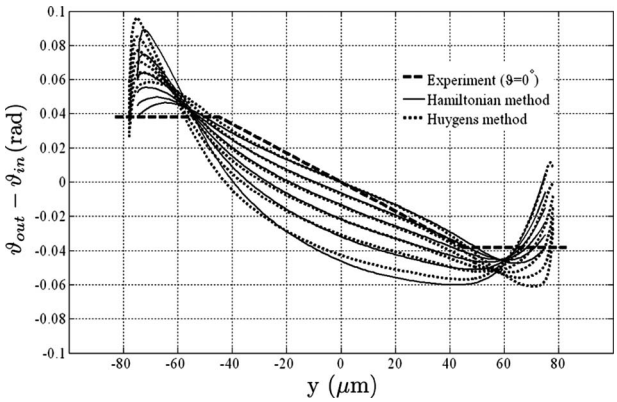

Fig. 9. Ray-tracing results of the Huygens method (dashed curves) for $\vartheta_{\text{in}}=0°,\ldots,50°$, with steps of 10°. The experimental result for $\vartheta_{\text{in}}=0°$ is also depicted. The figure also shows the ray-tracing results of the Hamiltonian method applied to the averaged director profile depicted in Fig. 8(b) (solid curves).

C. Hamiltonian Method Applied to the Averaged Director Profile

Next, we apply the Hamiltonian method to the averaged director profile $\hat{\mathbf{d}}(y)$ depicted in Fig. 8(b). With the propagation vector $\mathbf{s}$ at the liquid-crystal interface at $z=0$ μm as a boundary condition, we apply the Hamiltonian principle to calculate the curved ray path inside the liquid-crystal layer. The corresponding canonical equations for the position $\mathbf{r}$ and momentum $\mathbf{s}$ are given by

$$\frac{d\mathbf{r}(\tau)}{d\tau}=\nabla_s\mathcal{H}(\hat{\mathbf{d}}),$$

$$\frac{d\mathbf{s}(\tau)}{d\tau}=-\nabla_r\mathcal{H}(\hat{\mathbf{d}}), \tag{7}$$

with τ being a parameter that can be considered as time, and the partial derivatives read

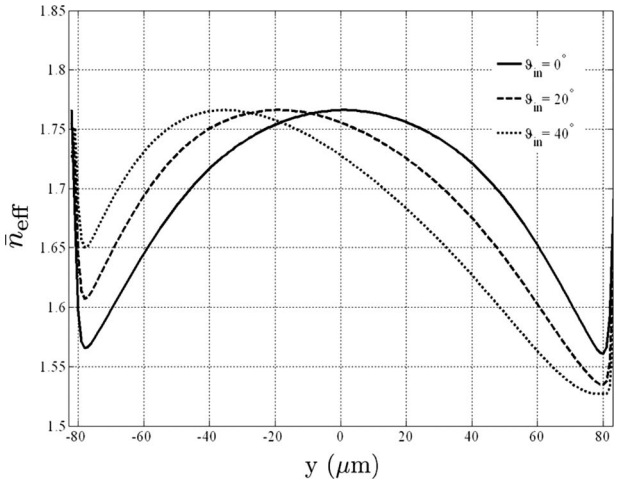

Fig. 10. Averaged effective index of refraction $\bar{n}_{\text{eff}}$ as a function of y for $\vartheta_{\text{in}}=0°$, 20°, and 40°.

$$\frac{\partial \mathcal{H}}{\partial i} = 2(n_e^2 - n_o^2)(\mathbf{s}\cdot\hat{\mathbf{d}})\left(s_x\frac{\partial \hat{d}_x}{\partial i} + s_y\frac{\partial \hat{d}_y}{\partial i} + s_z\frac{\partial \hat{d}_z}{\partial i}\right),$$

$$\frac{\partial \mathcal{H}}{\partial s_i} = 2n_o^2 s_i + 2(n_e^2 - n_o^2)(\mathbf{s}\cdot\hat{\mathbf{d}})\hat{d}_i, \quad i = x,y,z, \tag{8}$$

where $\mathcal{H}(\mathbf{r},\mathbf{s})$ is a scalar function describing the anisotropy of the extraordinary propagation vector $\mathbf{s}$ (cf. [19], p. 1269). The function $\mathcal{H}=0$ is called the refractive-index ellipsoid or optical indicatrix. These equations are a set of six coupled first-order differential equations for the vector components of $\mathbf{r}(\tau)$ and $\mathbf{s}(\tau)$. These differential equations can be solved with, e.g., the first-order Runge–Kutta method, also known as the Euler method (cf. [22], p. 704). At $z=12$ μm we calculate the refracted propagation vector $\mathbf{s}$ and the angle ϑ_{out}. The ray-tracing results are depicted in Fig. 9 (solid curves) together with the results of the Huygens method (dashed curves). Similar to the conclusion for the Huygens method, the lens effect according to the Hamiltonian method for $\vartheta_{\text{in}}=0°$ is slightly weaker than the lens effect observed in the experimental characterization. In addition, the Huygens and the Hamiltonian methods produce similar results, but the difference between them increases if ϑ_{in} increases. This is because when we apply the Hamiltonian method the ray paths of light rays are curved inside the liquid-crystal layer. Then the deflection of light rays from their original direction of propagation (at $z=0$ μm) increases with the optical path length inside the liquid-crystal layer and thus with angle ϑ_{in}.

For an angle of incidence ϑ_{in} smaller than approximately 40°, we conclude that the results of both the Huygens and the Hamiltonian methods are equivalent. In addition to this, we conclude that the Hamiltonian method predicts a stronger lens effect than the Huygens method for angles of incidence approximately above 40°.

D. Hamiltonian Method

Finally, we apply the Hamiltonian method to the simulated director profile $\hat{\mathbf{d}}(y,z)$ depicted in Fig. 8(a). This time, for $\vartheta_{in}=0°$, there is a good match between the experimental lens effect and the lens effect according to the ray-tracing results as can be seen in Fig. 11. For approximately $\vartheta_{\text{in}}\geq 10°$, the lens effects depicted in Fig. 11 (solid curves) are significantly stronger than the lens effects obtained from the averaged director profile (dashed curves). This is due to the fact that the numerical director profile in Fig. 8(a) is inhomogeneous in both the y and z directions. This means that, locally, the gradients in the index profile of the liquid crystal are higher and ray paths of light rays are converged more strongly.

Figure 12 shows $\vartheta_{\text{out}}(y)$ according to the experimental characterization, the Huygens method, and the Hamiltonian method for $\vartheta_{\text{in}}=20°$ [Fig. 12(a)] and for $\vartheta_{\text{in}}=40°$ [Fig. 12(b)]. From the results we can conclude that both the Huygens and the Hamiltonian methods are in good agreement with the experimental results in the region where $|y|\leq 45$ μm (active region of the GRIN lens). However, the discrepancies between the model and the experiment increase with the distance from the center

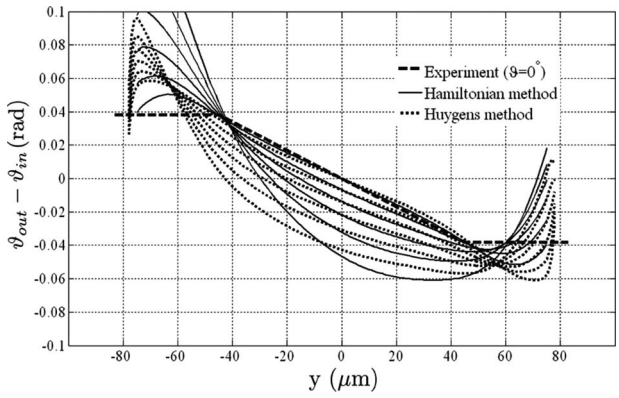

Fig. 11. Ray-tracing results of the Hamiltonian method applied to the director profile $\hat{\mathbf{d}}(y,z)$ depicted in Fig. 8(a) for $\vartheta_{\text{in}}=0°,\ldots,50°$, with steps of 10°. The results are presented together with the Huygens results of Fig. 9. The experimental result for $\vartheta_{\text{in}}=0°$ is also depicted. Clearly, the Hamiltonian method predicts a stronger lens action than the Huygens method does.

($y=0$ μm) and with increasing ϑ_{in}. This is because, for high values of ϑ_{in}, light rays entering the active region of the liquid-crystal GRIN lens ($|y|\leq 45$ μm) can penetrate the region close to the line electrodes ($|y|>45$ μm). These observations can be explained in view of two effects. On one hand, the properties of the liquid crystal in the region of the line electrodes are not well defined, since the liquid crystal does not align properly along the electric field lines. On the other hand, the simulated director profile is

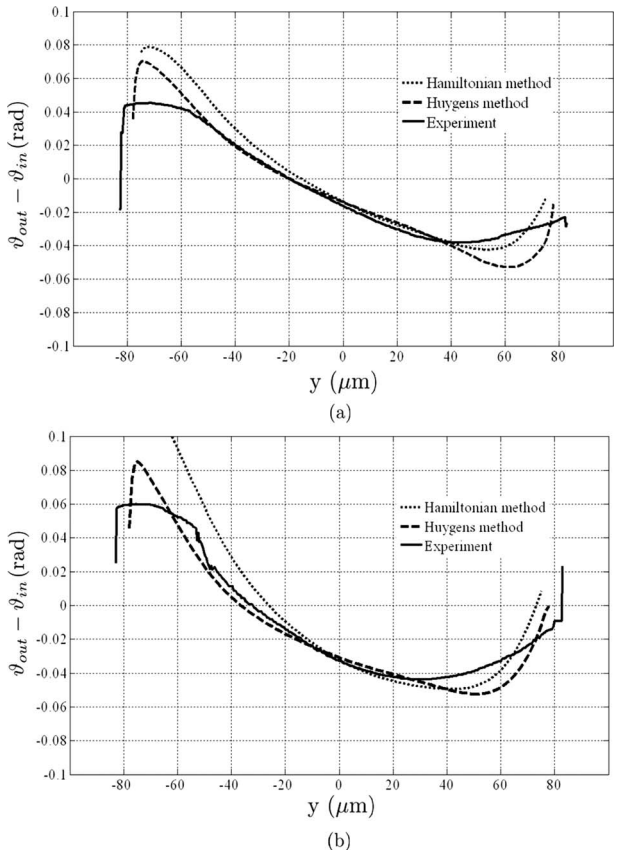

Fig. 12. In (a), ray-tracing results of the Hamiltonian method and the Huygens method are compared with the experimental result for $\vartheta_{\text{in}}=20°$. In (b), $\vartheta_{\text{in}}=40°$.

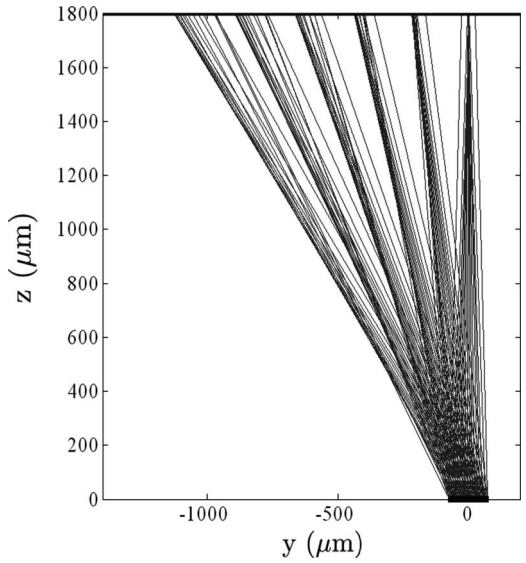

Fig. 13. Ray paths of light rays in the glass cover plate for incident plane waves with $\vartheta_{in}=0°,\ldots,50°$ with steps of 10°. The light rays for $\vartheta_{in}=0°$ are focused in the pixel plane at approximately $z=1800$ μm. The lens action for oblique angles of incidence decreases with ϑ_{in}.

prone to errors close to the line electrodes, since there the electric field changes rapidly per unit length.

Finally Fig. 13 shows the ray paths of light rays for $\vartheta_{in}=0°,\ldots,50°$ with steps of 10°. The light rays for $\vartheta_{in}=0°$ are deflected by the GRIN lens structure and are focused in the pixel plane at approximately $z=1800$ μm. Clearly, the lens action of the GRIN structure decreases with the angle of incidence: for angles of approximately 30° and higher, the lens action has become significantly weaker. At 30°, the light spot at the pixel plane is 100 μm while the width of a subpixel is 85 μm. Then the light spot at the pixel plane covers two neighboring pixels of the LCD. As a result, for high viewing angles two neighboring views (see Fig. 1) have too much overlap compromising the 3D performance.

6. CONCLUSIONS

We have investigated the angular-dependent optical behavior of an advanced liquid-crystal GRIN lens structure. This GRIN lens structure is designed for application in switchable autostereoscopic 2D/3D displays and is equivalent to the functionality of a switchable lenticular.

To model the angular-dependent optical properties of the liquid-crystal GRIN lens structure, we have used the Huygens and the Hamiltonian methods. The Huygens method is based on a one-dimensional approach. This is a fair approximation since the ratio between the thickness and the lens pitch is much smaller than 1 (0.07). In contrast to the Huygens method, the Hamiltonian method takes into account the full inhomogeneous material properties of the liquid crystal.

The director profile of the advanced liquid-crystal GRIN lens structure has been calculated in two different ways. First, an averaged director profile has been calculated from experimental results. This has been done by applying the Huygens method in reverse. Second, a numerical director profile has been simulated using LCD Master. This numerical director profile is inhomogeneous in two dimensions.

Based on the ray-tracing simulations, we conclude that the lens action of the advanced GRIN lens structure decreases with increasing angle of incidence. Moreover, the difference between the Hamiltonian and the Huygens methods increases with increasing angle of incidence. This is due to the fact that in contrast to the Huygens method, the Hamiltonian method incorporates the fact that ray paths of light rays are curved.

The regions near the line electrodes have relatively high gradients in the liquid-crystal profile. In theory, these regions are appropriate to visualize the difference between the Huygens and the Hamiltonian methods. However, in these specific regions, the liquid crystal does not align properly along the electric field lines and therefore does not contribute to the desired lens action. In addition, the simulated numerical director profile is prone to errors in the region of the line electrodes. Therefore both the theoretical and experimental results are inaccurate in these regions.

From the ray-tracing results we conclude that, for small viewing angles in a 3D display, the light from the pixel plane is well collimated by the GRIN lens structure. For large viewing angles of approximately 30° and higher, the lens action of the GRIN lens is significantly weaker. At 30°, the light spot at the pixel plane is 100 μm while the width of a subpixel is 85 μm. Then the 3D performance of the 3D display is compromised. This is an important reason why the application of liquid-crystal GRIN lenses in 3D displays for high viewing angles is still in need of further research. The general approach and the advanced ray-optics analysis procedures presented in this paper form a useful tool in the search for improvements and enable a better understanding of the liquid-crystal technology discussed.

ACKNOWLEDGMENTS

L. H. C. Kusters and H. B. J. Plasschaert are gratefully thanked for their valuable contributions. We also thank Fetze Pijlman and Siebe de Zwart for their contributions and fruitful discussions.

REFERENCES

1. D. F. McAllister, *Stereoscopic Computer Graphics and Other True 3D Technologies* (Princeton U. Press, 1993).
2. S. T. de Zwart, W. L. IJzerman, T. Dekker, and W. A. M. Wolter, "A 20″ switchable auto-stereoscopic 2D/3D display," in *11th International Display Workshop* (2004), pp. 1459–1460.
3. W. L. IJzerman, S. T. de Zwart, and T. Dekker, "Design of 2D/3D switchable displays," J. Soc. Inf. Disp. **36**, 98–101 (2005).
4. D. K. G. de Boer, M. G. H. Hiddink, M. Sluijter, O. H. Willemsen, and S. T. de Zwart, "Switchable lenticular-based 2D/3D displays," Proc. SPIE **6490**, 64900R (2007).
5. M. P. C. M. Krijn, S. T. de Zwart, D. K. G. de Boer, O. H. Willemsen, and M. Sluijter, "2D/3D displays based on switchable lenticulars," J. Soc. Inf. Disp. **16**, 847–855 (2008).

6. H. Hong, S. Jung, B. Lee, and H. Shin, "Electric-field-driven LC lens for 3-D/2-D autostereoscopic display," J. Soc. Inf. Disp. **17**, 399–406 (2009).
7. SHINTECH, Inc., http://www.shintech.jp.
8. AUTRONIC MELCHERS GmbH, http://www.autronic-melchers.com.
9. S. Sato, "LC-lens cell with variable focal length," Jpn. J. Appl. Phys. **18**, 1679–1684 (1979).
10. D. W. Berreman, "Variable-focus LC-lens system," U.S. patent 4,190,330 (February 26, 1980).
11. S. T. Kowel, D. S. Clevery, and P. G. Kornreich, "Focusing by electrical modulation of refraction in a liquid crystal cell," Appl. Opt. **23**, 278–289 (1984).
12. P. F. Brinkley, S. T. Kowel, and C. Chu, "Liquid crystal adaptive lens: beam translation and field meshing," Appl. Opt. **27**, 4578–4586 (1988).
13. J. S. Patel and K. Rastani, "Electrically controlled polarization-independent liquid-crystal Fresnel lens arrays," Opt. Lett. **16**, 532–534 (1991).
14. A. F. Naumov, M. Y. Loktev, I. R. Guralnik, and G. Vdovin, "Liquid-crystal adaptive lenses with modal control," Opt. Lett. **23**, 992–994 (1998).
15. H. Ren and S. T. Wu, "Adaptive liquid crystal lens with focal length tunability," Opt. Express **14**, 11292–11298 (2006).
16. G. E. Nevskaya and M. G. Tomilin, "Adaptive lenses based on liquid crystals," J. Opt. Technol. **75**, 563–573 (2008).
17. C. Jenkins, R. Bingham, K. Moore, and G. D. Love, "Ray equation for a spatially variable uniaxial crystal and its use in the optical design of liquid-crystal lenses," J. Opt. Soc. Am. A **24**, 2089–2096 (2007).
18. M. Kline and I. W. Kay, *Electromagnetic Theory and Geometrical Optics* (Wiley, 1965).
19. M. Sluijter, D. K. G. de Boer, and J. J. M. Braat, "General polarized ray-tracing method for inhomogeneous uniaxially anisotropic media," J. Opt. Soc. Am. A **25**, 1260–1273 (2008).
20. T. C. Kraan, T. van Bommel, and R. A. M. Hikmet, "Modeling liquid-crystal gradient-index lenses," J. Opt. Soc. Am. A **24**, 3467–3477 (2007).
21. R. A. M. Hikmet, T. van Bommel, T. C. Kraan, L. H. C. Kusters, S. T. de Zwart, O. H. Willemsen, and M. P. C. M. Krijn, "Beam-shaping device," U.S. patent pending WO/2008/126049A1 (2008).
22. W. H. Press, S. A. Teukolsky, W. T. Vetterling, and B. P. Flannery, *Numerical Recipes in FORTRAN: The Art of Scientific Computing* (Cambridge Univ. Press, 1992).
23. The Merck Group, Chemicals, www.merck.de.